

African Land-Cover Classification Using Satellite Data

Compton J. Tucker, John R. G. Townshend, Thomas E. Goff

Accurate, timely information on the distribution of vegetation on the earth's surface is a requisite for understanding how changes in land cover affect phenomena as diverse as the atmospheric CO₂ concentrations, terrestrial primary productivity, the hydrologic cycle, and the energy balance at the surface-atmosphere interface. Such information about

is apparent in the maps of, and ancillary texts on, the vegetation of Africa (1, 2) and is further illustrated by the widely varying estimates of the surface area of world terrestrial ecosystems (3, 4). An alternative approach is to use satellite remote-sensing data with its synoptic overview as a basis for mapping. In numerous studies such remotely sensed

Summary. Data from the advanced very-high-resolution radiometer sensor on the National Oceanic and Atmospheric Administration's operational series of meteorological satellites were used to classify land cover and monitor vegetation dynamics for Africa over a 19-month period. There was a correspondence between seasonal variations in the density and extent of green-leaf vegetation and the patterns of rainfall associated with the movement of the Intertropical Convergence Zone. Regional variations, such as the 1983 drought in the Sahel of western Africa, were observed. Integration of the weekly satellite data with respect to time for a 12-month period produced a remotely sensed estimate of primary production based upon the density and duration of green-leaf biomass. Eight of the 21-day composited data sets covering an 11-month period were used to produce a general land-cover classification that corresponded well with those of existing maps.

vegetative cover is also required in determining the rates of change of the earth's biotic resources and the ways in which land use is adjusting to increasing demands on these resources.

Traditionally, the principal source of such information has been vegetation mapping by ground survey. If large areas are surveyed, it is inevitable that the observations of many different observers must be synthesized, which introduces all the problems of reconciling disparate observations. The magnitude of the task

data have been used to accurately map vegetation, crops, and other land-cover types (5). The majority of these studies have used Landsat data, and none of them have attempted classification at continental scales.

One reason why it has not been possible to accomplish continental-scale vegetation classifications from Landsat data is because of its 80-m spatial resolution. This spatial resolution of the Landsat multispectral scanner system (MSS) and associated 185- by 185-km scene makes it necessary to accumulate a substantial quantity of data (about 1100 individual Landsat images) to cover an area as large as Africa. Thus logistical and financial

problems are sizeable if a continental-scale analysis is to be performed in a digital mode with Landsat MSS data.

It is highly desirable to collect several images each year to overcome cloud cover problems while monitoring changes in vegetation over time (6). Multiple imaging within a given year allows classification to be based on phenological changes in different vegetation types (5). Such an approach becomes essential in Africa if land-cover types are to be spectrally discriminated because of the asynchronous responses of vegetation to seasonal rainfall north and south of the equator and the marked wet and dry seasons.

As an alternative to Landsat images, we propose the use of advanced very-high-resolution radiometer (AVHRR) data from the National Oceanic and Atmospheric Administration (NOAA) meteorological satellites. Such data have been shown to have significant potential for assessing and mapping vegetation over relatively modest areas (7, 8), and similar levels of classification accuracy have been reported between Landsat MSS and NOAA AVHRR data for some natural vegetation types (9). AVHRR data have a much coarser resolution (1 and 4 km at nadir) and hence a lower data volume and cost than Landsat MSS data, and their temporal resolution is much higher with 4-km imagery globally available on a daily basis.

It should be stressed that we are attempting to map physiognomic types or vegetation formations according to land-cover criteria rather than any alternative criteria that have been proposed, such as environmental characteristics, phylogeny, or individual form features (10). Our approach is based upon satellite data collected daily for 19 months for the continent of Africa and uses the satellite-recorded multitemporal characteristics of land cover for large-scale classification purposes.

Methods

The AVHRR sensor of the NOAA satellites was chosen to provide the data (11). Earlier data from this sensor on-

C. J. Tucker and T. E. Goff are with the NASA Goddard Space Flight Center, Greenbelt, Maryland 20771. J. R. G. Townshend is with the Geography Department of the University of Reading, Reading, Berkshire, United Kingdom.

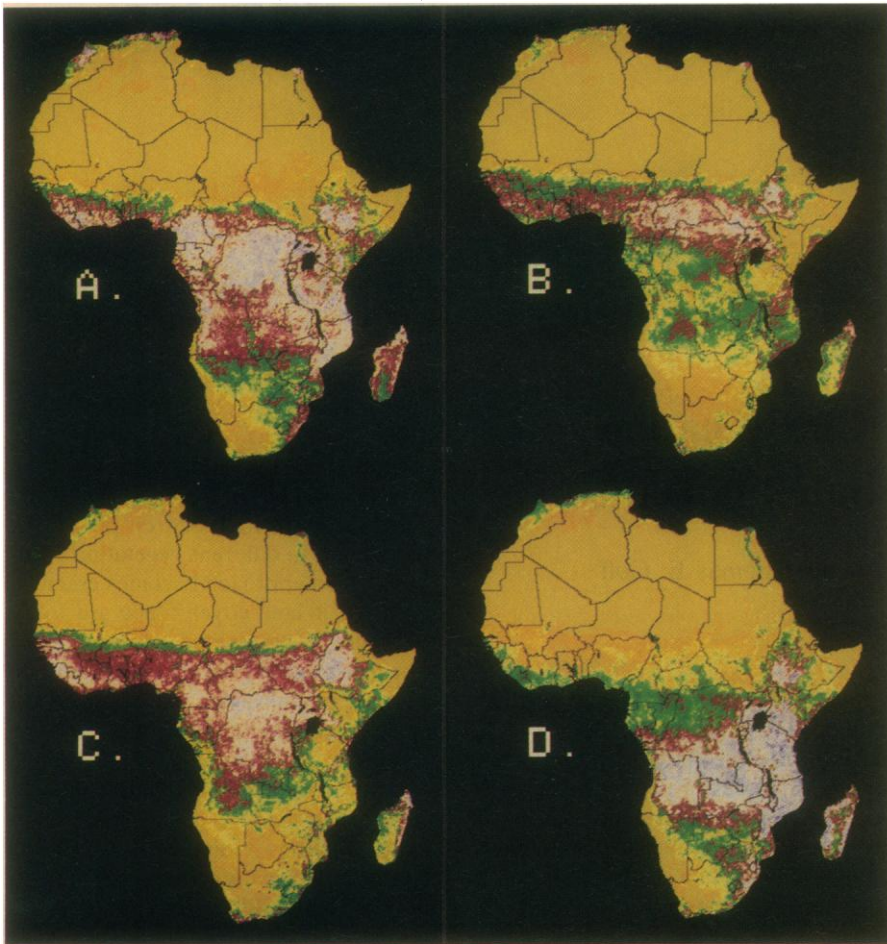


Fig. 1. The spectral vegetation index from Africa for four selected 21-day periods: (A) 12 April to 2 May 1982; (B) 5 to 25 July 1982; (C) 27 September to 17 October 1982; and (D) 20 December 1982 to 9 January 1983. These data are the maximum normalized-difference values from 3 weeks of the NOAA global vegetation index product and have a spatial resolution of 15 km at the equator. The tan and brown colors represent no green leaf vegetation, and the reds and purples represent the highest amounts. Values for green-leaf vegetation range from approximately 0.05 to 0.60.

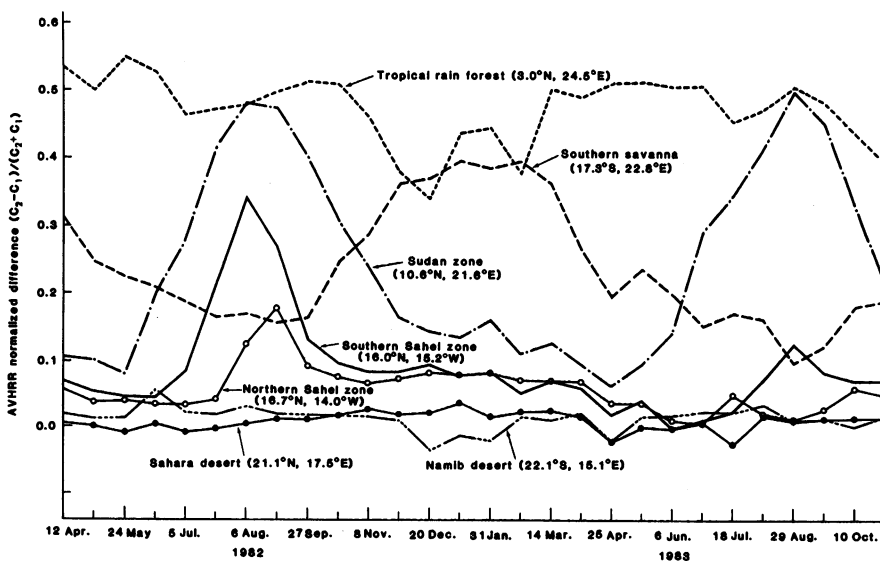


Fig. 2. The spectral vegetation index from April 1982 to November 1983 at seven African locations. One value is plotted per location for each 21-day period. The first day of each 21-day period is indicated on the X-axis (that is, 12 April is actually 12 April to 2 May 1982). Each value plotted represents the average of nine picture elements or approximately 2500 km².

board the Television and Infrared Observing Satellite (TIROS) were unsatisfactory because of the overlap between the visible and near-infrared bands, which made it impossible to produce a spectral green vegetation index (12). Global-area coverage (GAC) data with a 4-km resolution were chosen rather than the finer resolution local-area coverage (LAC) data with a 1-km resolution, since the 4-km data were available daily for the whole continent.

The 4-km GAC data are partly resampled 1-km LAC data; the first four 1-km picture elements are averaged, and this average is then used to represent a 3 by 5 picture element block (11). The GAC data are tape-recorded onboard the satellite and subsequently transmitted to receiving stations in either Virginia or Alaska.

Fourteen NOAA-7 orbits cover the entire world each day. The daytime global AVHRR 4-km channel 1 (C_1) and channel 2 (C_2) data are mapped by NOAA into 1024 by 1024 element arrays for the Northern Hemisphere and Southern Hemisphere every day. These data, available from NOAA on a daily basis or as a weekly composite, have a grid cell size of ~15 km at the equator and ~30 km at the poles (13). Ratio or linear combinations of the C_1 and C_2 radiances can be used to generate spectral indices that are used to nondestructively estimate the green-leaf biomass or green-leaf area of plant canopies (14). Recent researchers have reported very high correlations between the spectral green-leaf indices and the photosynthetically active radiation absorbed by plant canopies (15). Spectral green-leaf indices are also affected by off-nadir viewing, sun angle, background material reflectance, and atmospheric aerosols (16, 17), and these indices have an asymptotic or saturation response to high levels of green-leaf density (18).

The weekly global composite data are formed by selecting the highest spectral index for each grid cell location from the individual daily data for that week (13). We have taken the weekly C_1 and C_2 values from mid-April 1982 to November 1983, mapped them to a Mercator projection, formed the C_2/C_1 and $(C_2 - C_1)/(C_2 + C_1)$ ratios, and selected the highest value over a 3-week period for both spectral ratios for each grid cell location for Africa. Selecting the respective maximum spectral ratio for a 3-week period simultaneously minimized the effects of sun angle, off-nadir viewing, atmospheric path length and aerosols, and clouds, all of which can only decrease the spec-

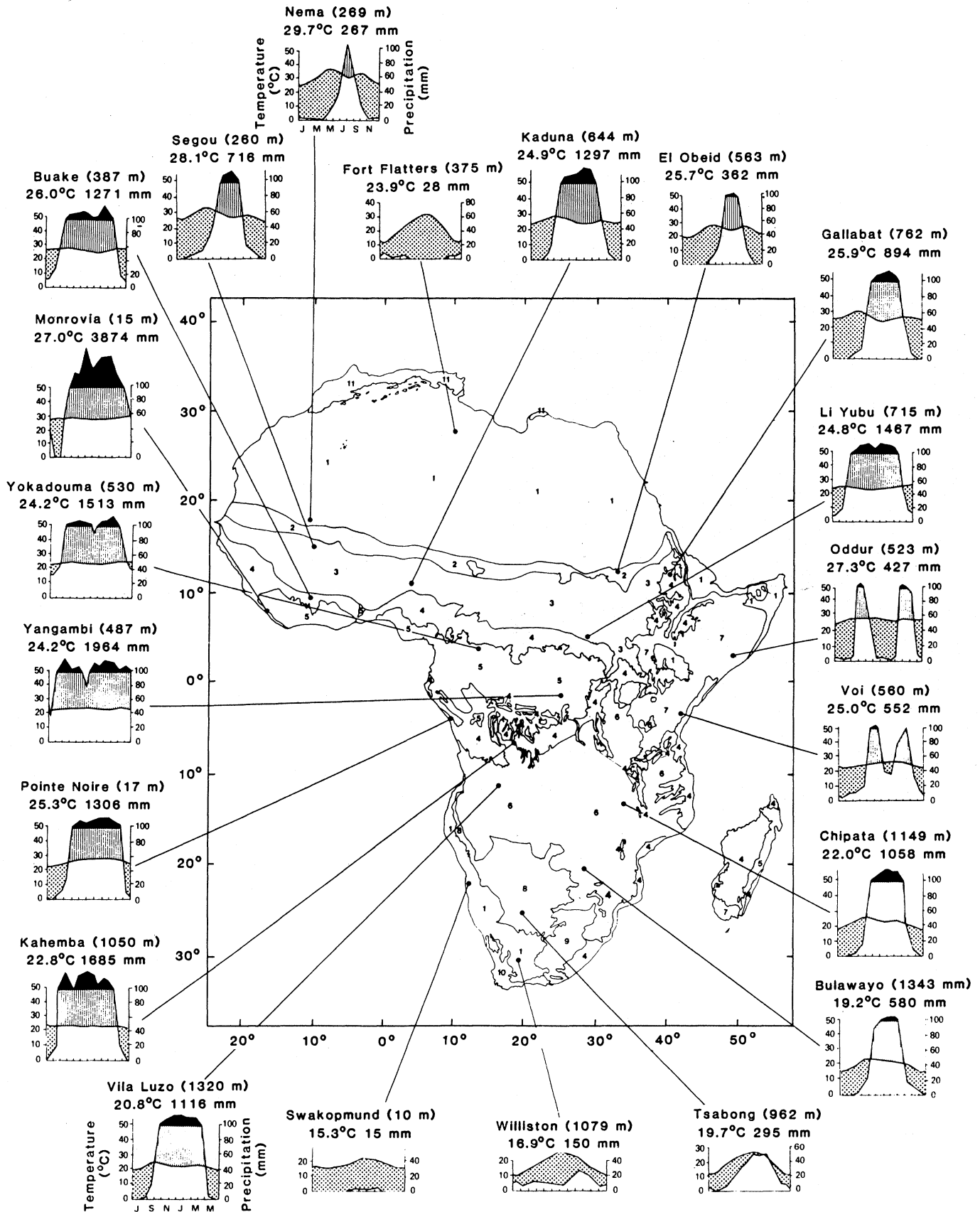


Fig. 3. Major vegetation types of Africa and Madagascar, simplified from White (1), with selected climate and elevation data after Walter and Lieth (23) and Walter *et al.* (24): 1, desert and semidesert shrubland-grassland; 2, wooded grassland and bushland (Sahel); 3, Sudanian woodland and grassland; 4, forest transition and mosaic; 5, forests; 6, woodlands, predominately Somalia-Masai; 8, Kalahari wooded grassland and bushland; 9, Karoo grassy shrubland and highveld grassland; 10, Cape and Karoo shrubland; and 11, Mediterranean vegetation. Climate data for selected sites are given in terms of the station name, elevation, average mean temperature (in degrees celsius), and average precipitation (in millimeters). The average monthly precipitation is plotted against time on a linear scale (stippled portion) and on a logarithmic scale (solid portion). Those months for which potential evapotranspiration exceeds precipitation are noted by the dotted areas. The average monthly temperature is also plotted against month. The months begin with January north of the equator and with July south of the equator.

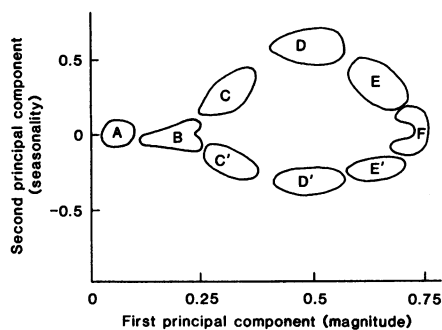


Fig. 4. A diagrammatic representation of the classification feature space formed between the first and second principal components from 21-day periods between April 1982 and February 1983. The first principal component was found to be highly similar to the integrated image appearing as the cover figure. The second principal component represents cover-type seasonality. Known surface areas were selected and used to label the feature space. The resulting labeling resulted in classes of water (A), desert (B), semiarid seasonal grasslands (C and C'), dry savannas (D and D'), wet savannas (E and E'), and tropical forest (F).

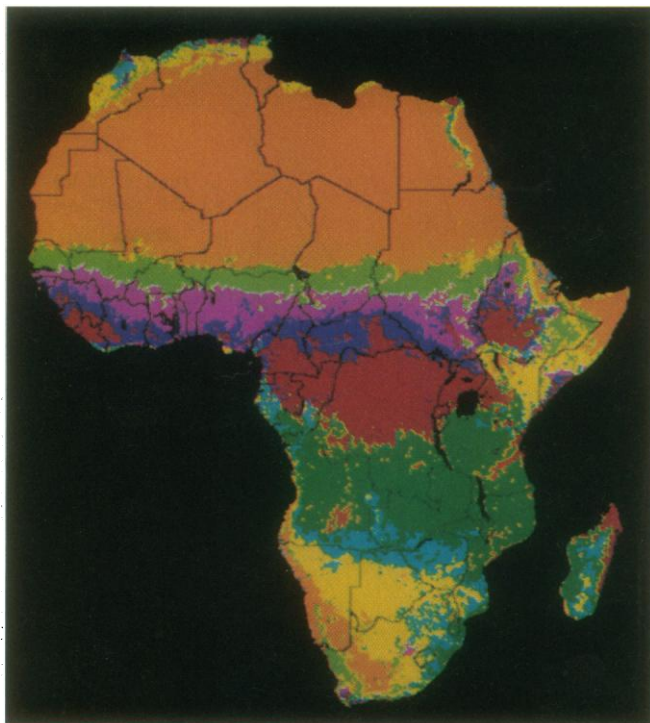


Fig. 5. Principal-components land-cover classification of Africa produced from eight 21-day composited images (12 April to 2 May 1982, 24 May to 13 June 1982, 5 to 25 July 1982, 6 to 26 August 1982, 27 September to 16 October 1982, 8 to 28 November 1982, 20 December 1982 to 10 January 1983, and 31 January to 19 February 1983). The feature space used to label land-cover classes is shown in Fig. 4. The tan areas are desert and semidesert, the light green areas semiarid wooded grassland and bushland, the purple areas Sudanian woodland and grassland, the dark blue areas interspersed tropical forest and grassland, the

red areas tropical rain forest and montane forest, the dark green areas woodland and especially Miombo woodland, the light blue areas bushland and thicket, and the yellow areas wooded grassland and deciduous bushland (see also Figs. 1 through 4).

Table 1. Net primary productivity and phytomass of terrestrial ecosystems. The adapted conversion of dry matter to carbon is 0.45 [from Ajtay *et al.* (3)].

Ecosystem type	Average net primary production of dry matter (g m ⁻² year ⁻¹)	Living phytomass (above and below ground) dry matter (g m ⁻²)
Forests		
Tropical humid	2,300	42,000
Tropical seasonal	1,600	25,000
Temperate evergreen	1,500	30,000
Temperate deciduous	1,300	28,000
Temperate woodlands (various)	1,500	18,000
Chaparral, maquis, bushland	800	7,000
Savanna		
Low tree-shrub savanna	2,100	7,500
Grass-dominated savanna	2,300	2,200
Dry savanna thorn forest	1,300	15,000
Dry thorny shrubs	1,200	5,000
Temperate grassland		
Moist	1,200	2,100
Dry	500	1,300
Desert and semidesert scrub		
Scrub-dominated	200	1,100
Sandy, hot, and dry	10	60

tral ratios (17). This process resulted in the selection of data that tend to occur near nadir, are largely cloud-free, and are characterized by low-aerosol conditions. A subjective appreciation of the results of this process may be gained from an inspection of Fig. 1, where no boundaries between satellite paths can be detected.

Compositing was performed on the Hewlett-Packard 1000 and Ramtek image-processing system at the Sensor Evaluation Branch, Goddard Space Flight Center. The importance of combining data over periods of time to minimize clouds, sun angles, directional reflectance, and atmospheric effects while maintaining the ability to record the temporal dynamics of vegetation must be stressed and is fundamental to the work we describe. The 3-week composites reduced cloud cover to less than 2 percent, with the balance of those clouds present occurring over coastal Gabon and Cameroon.

Multitemporal Dynamics of Green-Leaf Biomass

The ability to successfully composite daily satellite data on a continental scale provided the means to overcome the problems of extensive cloud cover in equatorial and other areas and the degrading effects caused by variations in sun angle, the atmosphere, and the satellite-target viewing geometry. Once cloud-free data were available at frequent intervals and the various degrading influences minimized, the large-scale multitemporal dynamics of green-leaf biomass could be recorded. Almost identical results were found for the C_2/C_1 ratio and the $(C_2 - C_1)/(C_2 + C_1)$ normalized difference vegetation index. Accordingly, we present only results from the normalized difference series of analyses and henceforth refer to the normalized difference as the spectral vegetation index.

Figure 1 illustrates the seasonal changes in green-leaf biomass as expressed in the spectral vegetation index for Africa at four selected 21-day intervals from April 1982 to January 1983. The movements of the Intertropical Convergence Zone were evident in the development of green-leaf biomass after periods of precipitation. Inspection of the 3-week data and their variation with time showed the growing season dynamics from seven selected locations (Fig. 2). The data presented in Fig. 1 represent four of the 28 3-week periods presented in Fig. 2 for seven selected locations. We

observed seasonal variation in our spectral vegetation index for almost all vegetated areas of Africa including tropical rain forest: deserts and semideserts were the only areas observed to be temporally invariant (Fig. 2). The nested curves for selected areas in the Sahel and Sudan zones, the southern savanna, and the tropical rain forest areas in Fig. 2 reflect the climatic conditions of the time period from April 1982 to November 1983 and are in general agreement with the 30-year climatic averages from similar African areas (Fig. 3). Higher values of the spectral vegetation index were observed during the 1982 rainy season in the West African Sahel than during 1983 (Fig. 2). This reduced spectral vegetation index in 1983 corresponded to a major drought in the northern and central Sahel zone in 1983 (19).

Seasonal variation in the spectral vegetation index was also observed in tropical rain forest, tropical seasonal forest, and savanna areas. Although this seasonality is expected for tropical seasonal forests and tropical savannas, it also occurs in most tropical rain forests (20, 21). Compared with rain forests on other continents, the African tropical rain forest is relatively dry and receives between 1600 to 2000 mm of rainfall per year. White (1) reported that areas receiving more than 3000 mm of rainfall per year are largely confined to coastal areas of Upper and Lower Guinea and that only a small part of the Zaire basin receives more than 2000 mm per year.

Not only is the rainfall in Africa lower than in rain forest regions elsewhere, but also its distribution throughout the year is uneven. Virtually nowhere in the African tropical rain forest is the mean monthly rainfall higher than 100 mm for every month of the year. South of the equator and toward the Atlantic coast but still at equatorial latitudes, the length and severity of the dry period increases (1). Consequently, the variation observed in the spectral vegetation index from African tropical rain forest areas is consistent with observed vegetation seasonality (22) and climatic data (23, 24) (Fig. 3). In addition, dry periods are more severe and frequent than the climate diagrams indicate, as the climate diagrams are based upon long-term mean values (1, 23, 24). Because of the marked wet and dry periods for African vegetation types, we observed the same spectral vegetation index for savanna areas as for tropical rain forest areas at times (Fig. 1A), higher spectral vegetation indices for tropical forests than for savanna areas at times (Fig. 1B), and higher spectral vegetation indices for savannas

than for tropical rain forest areas at other times (Figs. 1D and 2).

To quantify the yearly vegetation response for Africa we have integrated the spectral vegetation index with respect to time for the period from April 1982 to April 1983 (see cover). This technique has been used to approximate the primary production within a given vegetation type for the period of observation. This is so because the spectral vegetation index is highly correlated to the green-leaf biomass or projected green-leaf area (an indication of the area of the photosynthetic absorbing surface), which is one of several variables related to the rate of photosynthesis. Frequently collected spectral data, when integrated with respect to time, have been shown to be highly correlated to the total dry matter accumulation for wheat (6), corn (25), pastoral ecosystems (7), and crop yield (26). Essentially, the integrated spectral green-leaf indices are estimates of the integral intercepted visible radiation (15). Monteith (27) has reported that net production per unit of intercepted visible radiation was remarkably constant for crops as diverse as apples, barley, potatoes, and sugar beets in the United Kingdom. Although this integration technique has not been tested across different ecological zones or at continental scales, the data we report on are well suited for this purpose.

The integrated spectral index produced a zonation of Africa in which deserts and semideserts, dry savannas and dry grasslands, and forests and wet savanna were differentiated from each other (see cover). There is general qualitative agreement between the integrated image in the cover figure and various primary production data from different ecosystem types (Table 1). Tropical forest and tropical savanna have similar integrated index values. Primary production data (3, 20) and the fact that African tropical rain forests are relatively dry as compared to rain forest in other continents (1) tend to support the integrated data in the cover figure (Table 1). We acknowledge a range of primary production estimates (28). Detailed quantitative verification of the zonations presented in the cover figure will be a tedious and time-consuming process.

Land-Cover Classification

There is a high correlation between the integrated image (cover figure) and the major land-cover types found in Africa (Fig. 3). For example, the highest values correspond to the forest and wetter sa-

vanna areas, and the lowest to desert and semidesert areas. These relationships, along with the distinctive temporal variation of different cover types (Fig. 2), suggested that a continent-wide land-cover classification should prove feasible and the following procedure was adopted. From the 28 cloud-free geographically referenced data sets, eight dates between April 1982 and February 1983 were used for classification purposes. These were chosen since their spacing provided an opportunity to use seasonal phenological changes in green-leaf biomass to classify the land cover. We chose the spectral vegetation index as the variable used to define the feature space for two reasons. (i) For a given vegetation type, this index is related to variables such as the projected green-leaf area, green-leaf biomass, or the intercepted fraction of photosynthetically active radiation. (ii) Use of the spectral vegetation index meant that differences in radiance received at the sensor as a result of differences in solar elevation would be largely eliminated.

A principal-components classification procedure was used for eight 3-week periods of data between April 1982 and February 1983 (29). The spectral vegetation index was the variable used from time 1 to time 8. The n principal components P are related to the original variables by

$$P_i = \sum a_{ij} NDVI_j \quad (1)$$

$$i = 1, 8$$

$$j = 1, 8$$

where a_{ij} are the eigenvectors ranked in order corresponding to the size of the eigenvalues and $NDVI$ is a spectral vegetation index for time j . Each eigenvector represents the relative contribution of each time period to the principal component and is obtained by solving the equation

$$C\lambda_{ij} = a_{ij}\lambda_i \quad (2)$$

where C is the covariance matrix of the spectral vegetation indices for the nine time periods and λ_{ij} is the positive eigenvalue representing the variance of each principal component (29). The first eight principal components were generated and the first and second principal components used for classification purposes.

The first principal component had near equal eigenvector weightings for all eight dates and has been reported to be nearly identical to the integrated spectral vegetation index (30). The second principal component showed a quasi-sinusoidal structure with marked negative and high positive values in the dry and wet sea-

sons, respectively, in both hemispheres, reflecting the asynchronous sequence of rainy seasons in the two hemispheres of Africa. Areas of the Sudan and Sahel zones had high positive values while similar areas of vegetation in southern Africa had low negative values, and desert areas showed no seasonal changes and had second principal component values close to zero (Fig. 4). We selected areas of known vegetation types for classification training-site purposes on the basis of the African field experience of the authors and agreement among the various vegetation maps (1, 2). These training areas, which represented less than 5 percent of the African surface area, were used to label the feature space formed between the first and second principal components for each pixel of the African data. Boundaries of the various vegetation types were determined on the basis of the location of the training areas in the feature space and the classification image produced (Fig. 5).

Several qualifications need to be stated concerning the land-cover map shown in Fig. 5. We stress that we did not primarily attempt definitive or even quasi-definitive land-cover classifications of Africa but instead attempted to evaluate the feasibility of using NOAA-7 AVHRR data for this purpose. No formal performance evaluation has been carried out. Our evaluation has been hindered by the substantial lack of agreement among existing vegetation maps for many locations of Africa. We therefore have no quantitative basis for comparison as yet. Field checking will clearly be extremely time-consuming, and a satisfactory sample of test sites may take several years to collect. Nevertheless, we intend to carry out such a field program. At present, we must rely on the African field experience of ourselves and colleagues along with a qualitative comparison with existing vegetation maps such as that shown in Fig. 3. Comparisons with such maps suggests a considerable measure of agreement, although certain errors can be noted. The classification of desert north of the equator includes both deserts and other semiarid zones with precipitation up to approximately 300 mm/year (Fig. 5). As such, this includes a portion of the Sahelian zone (200 to 400 mm/year). The extent of closed-canopy forest in eastern Africa is probably overestimated. In coastal Gabon and Cameroon the amount of rain forest may have been somewhat underestimated because of the remarkably high frequency of clouds and haze in the early afternoon in this area.

The classification of vegetation on the Mediterranean coast is described in the same terms as that in the rest of the map. We also recognize the error introduced by using data from a 1-year period, which does not account for yearly variation in climate. This is evident in Fig. 2 for the Sahel zone between 1982 and 1983. In future more detailed mapping we plan to use multiyear data accompanied by labeling on the basis of the known differences in the assemblage of vegetation formations.

Conclusions

The mapping of the AVHRR images to a common geographically referenced data base provided the basis for image compositing to produce near cloud-free images of the entire African continent, in which atmospheric and satellite-target viewing geometry effects were minimized. A spectral vegetation index was calculated to allow the green-leaf dynamics of the African surface to be monitored for the whole of Africa and was used to construct a continent-wide land-cover classification based on the multi-temporal responses of land cover. There was qualitative agreement with the reported distribution of vegetation (1, 2) for most of the continent. In some areas errors occurred, and thus refinements to existing classification methods need to be developed. In particular, data from several years are needed to overcome yearly climatic variation. Despite these important qualifications, the results suggest the prospect for internally consistent mapping and repeated monitoring of the main cover types of continental areas based on the use of multitemporal coarse-resolution satellite data.

References and Notes

1. F. White, *The Vegetation of Africa* (Unesco, Paris, 1983).
2. *Vegetation Map of the Mediterranean Region* (Unesco, Paris, 1968); S. R. Eyre, *Vegetation and Soils, a World Picture* (Arnold, London, 1963); Committee for the World Atlas of Agriculture, *World Atlas of Agriculture* (Agostini-Novare, Italy, 1969); R. W. J. Keay, *Vegetation Map of Africa* (Clarendon, Oxford, 1959).
3. G. L. Ajtay, P. Ketner, P. Duvigneaud, in *The Global Carbon Cycle*, B. Bolin, E. T. Degens, S. Kempe, P. Ketner, Eds. (Scientific Committee on Problems of the Environment Report 13) (Wiley, New York, 1979), p. 129.
4. N. I. Bazilevich, Y. L. Rodin, N. N. Rozov, *Sov. Geogr.* 12, 293 (1971); H. J. M. Bowen, *Trace Elements in Biochemistry* (Academic Press, New York, 1966); E. S. Deevey, *Sci. Am.* 203, 195 (1960); F. B. Golley, in *Ecosystem Structure and Function*, J. A. Weins, Ed. (Oregon Univ. Press, Corvallis, 1972), p. 69; H. Lieth, *Geographisch Taschenbuch* (Steiner, Wiesbaden, 1964); G. Schmidt, *Vegetationsgeographie auf Ökologisch-Soziologischer Grundlage* (Teubner, Leipzig, 1969); H. L. Shantz, *Ecology* 35, 143 (1960); L. D. Stamp, *Our Developing World* (Faber and Faber, London, 1960); R. H. Whittaker, *Communities and Ecosystems* (Macmillan, Toronto, 1970); _____ and G. E. Likens, in *Carbon and the Biosphere*, G. M. Woodwell and E. V. Pecan, Eds. (National Technical Information Services, Springfield, Va., 1973), p. 281; R. H. Whittaker and G. E. Likens, in *Primary Production of the Biosphere*, H. Lieth and R. H. Whittaker, Eds. (Springer, Berlin, 1975), p. 305.
5. M. C. Bauer, J. E. Cipra, P. E. Anuta, J. E. Etheridge, *Remote Sensing Environ.* 9, 77 (1979); M. D. Fleming, J. S. Berkebile, R. M. Hoffer, *LARS Note 72475* (Laboratory for Applications of Remote Sensing, West Lafayette, Ind., 1975); C. O. Justice, in *Proceedings of the American Society of Photogrammetry Fall Meeting* (Falls Church, Va., 1978), p. 303.
6. C. J. Tucker, B. N. Holben, J. H. Elgin, J. E. McMurtrey, *Remote Sensing Environ.* 11, 171 (1981); J. K. Aase and F. H. Siddoway, *ibid.*, p. 267.
7. C. J. Tucker, C. Vanpraet, E. Boerwinkel, A. Gaston, *ibid.* 13, 461 (1983).
8. R. C. Cicone and M. D. Metzler, *ibid.* 14, 257 (1984); T. I. Gray and D. G. McCrary, *AgRI-STARS [Agriculture and Resources Inventory Surveys through Aerospace Remote Sensing] Rep. EW-NI-04042* (NASA, Houston, 1981); S. R. Schneider and D. F. McGinnis, in *Proceedings of the 1982 Conference on Machine Processing of Remotely Sensed Data* (Laboratory for Applications of Remote Sensing, West Lafayette, Ind., 1982), p. 281; _____, J. A. Gatlin, *NOAA Tech. Rep.* 84 (1981); J. R. G. Townshend and C. J. Tucker, in *Matching Remote Sensing Technologies and Their Applications* (Remote Sensing Society, London, 1981), p. 97; C. J. Tucker, J. A. Gatlin, S. R. Schneider, M. A. Kuchinos, in *Proceedings of Conference on Remote Sensing of Arid and Semi-Arid Lands* (Univ. of Michigan Press, Ann Arbor, 1982), p. 973.
9. J. G. Gervin, A. G. Kerber, R. G. Witt, Y. C. Lu, R. Sekhon, in *Proceedings of 17th International Symposium on Remote Sensing of the Environment* (Univ. of Michigan Press, Ann Arbor, 1983), p. 1067; J. P. Ormsby, *IEEE Trans. Geosci. Remote Sensing GE-20*, 262 (1982).
10. D. J. de Laubenfels, *Mapping the World's Vegetation* (Syracuse Univ. Press, Syracuse, 1975).
11. K. A. Kidwell, *NOAA Polar Orbiter Specifications* (Department of Commerce, Washington, D.C., 1979). The characteristics of the NOAA-6, NOAA-7, and NOAA-8 AVHRR's may be summarized as follows. The satellites have a sun-synchronous orbit with 102° inclination, 101.6-minute orbital period, and overpass times of 0730 and 1930 hours (NOAA-6 and NOAA-8) and 1430 and 0230 hours (NOAA-7). There are 1024 quantizing levels (10 bits). The field of view is 1.1 km at nadir. The swath width is 2700 km (2048 pixels). The spectral channels are located at 0.55 to 0.68 μm , 0.73 to 1.1 μm , 3.5 to 3.9 μm , 10.5 to 11.5 μm , and 11.5 to 12.5 μm .
12. C. J. Tucker, *Photogramm. Eng. Remote Sensing* 44, 1369 (1978). The AVHRR on NOAA-6, launched in June 1979, was the first AVHRR instrument to have bands from 0.55 to 0.68 μm and 0.73 to 1.1 μm . Earlier satellites in the TIROS-N series had AVHRR instruments with bands from 0.55 to 0.90 μm and 0.73 to 1.1 μm , which made calculation of any spectral green-vegetation index impossible.
13. J. D. Tarpley, S. R. Schneider, R. L. Money, *J. Climate Appl. Meteorol.* 23, 491 (1984).
14. C. F. Jordan, *Ecology* 50, 663 (1969); R. L. Pearson and L. D. Miller, in *Proceedings of the 8th International Symposium on Remote Sensing in the Environment* (Univ. of Michigan Press, Ann Arbor, 1972), p. 1357; J. W. Rouse, R. H. Haas, J. A. Schnell, D. W. Deering, in *3rd Symposium on Significant Results Obtained with ERTS-1* (NASA Special Publication SP-351, Washington, D.C., 1973), p. 309; J. E. Colwell, *Remote Sensing Environ.* 3, 175 (1974); E. L. Maxwell, *Photogramm. Eng. Remote Sensing* 42, 1173 (1976); S. J. McNaughton, *Science* 191, 92 (1976); C. J. Tucker, *Remote Sensing Environ.* 9, 127 (1979); C. L. Wiegand, A. J. Richardson, E. J. Kanemasu, *Agron. J.* 71, 336 (1979); B. N. Holben, C. J. Tucker, C. J. Fan, *Photogramm. Eng. Remote Sensing* 46, 651 (1980); D. S. Kimes, B. L. Markham, C. J. Tucker, J. E. McMurtrey, *Remote Sensing Environ.* 11, 401 (1981); J. K. Aase and F. H. Siddoway, *Agron. J.* 72, 149 (1980); P. J. Curran and E. J. Milton, *Int. J. Remote Sensing* 4, 246 (1983); P. J. Curran, *Philos. Trans. R. Soc. London* 309, 257 (1983); D. S. Bartlett and V. Klemas, *Environ. Manage.* 4, 337 (1980); J. S. Ahlrichs, M. E. Bauer, M. M. Hixson, C. S. T.

- Daughtry, D. W. Crecelius, in *Proceedings of the International Symposium on Remote Sensing for Observation and Inventory of Earth Resources and the Endangered Environment*, G. Hildebrandt and H. J. Boehnel, Eds. (International Society of Photogrammetry, Freiburg, 1979), p. 629; C. S. T. Daughtry, M. E. Bauer, D. W. Crecelius, M. M. Hixson, *AgRISTARS Rep. SR-PO-00458* (NASA, Houston, 1980); T. W. Brakke, E. T. Kanemasu, J. L. Steiner, F. T. Ulaby, E. Wilson, *Remote Sensing Environ.* **11**, 207 (1981); C. P. Perry and L. F. Lautenschlager, *ibid.* **14**, 169 (1984).
15. M. Kumar and J. L. Monteith, in *Plants and the Daylight Spectrum*, H. Smith, Ed. (Academic Press, London, 1982), p. 133; J. L. Hatfield, G. Asrar, E. T. Kanemasu, *Remote Sensing Environ.* **14**, 65 (1984); C. L. Wiegand and A. J. Richardson, *Agron. J.* **76**, 543 (1984); C. S. T. Daughtry, K. P. Galio, M. E. Bauer, *ibid.* **75**, 527 (1983).
16. J. V. Dave, *Remote Sensing Environ.* **10**, 87 (1980); *ibid.* **11**, 37 (1981); P. N. Slater and R. D. Jackson, *Appl. Opt.* **21**, 3923 (1982); R. D. Jackson, P. N. Slater, P. J. Pinter, *Remote Sensing Environ.* **13**, 187 (1983); M. J. Duggin, *Appl. Opt.* **16**, 521 (1977); D. S. Kimes, J. A. Smith, K. J. Ranson, *Photogramm. Eng. Remote Sensing* **46**, 1563 (1980); J. A. Kirchner, D. S. Kimes, J. E. McMurtrey, *Appl. Opt.* **21**, 3766 (1982); J. A. Kirchner and C. C. Schnetzler, *Int. J. Remote Sensing* **2**, 253 (1981); D. S. Kimes and J. A. Kirchner, *Appl. Opt.* **21**, 4119 (1982); K. L. Coulson, *ibid.* **5**, 905 (1966); F. D. Eaton and I. Dirmhirn, *ibid.* **18**, 994 (1979); K. T. Kriebel, *ibid.* **17**, 253 (1978); K. J. Ranson, V. C. Vanderbilt, L. L. Biehl, B. F. Robinson, M. E. Bauer, in *Proceedings of the 15th International Symposium on Remote Sensing in the Environment* (Univ. of Michigan Press, Ann Arbor, 1981), p. 853; D. Kimes, *Appl. Opt.* **22**, 1364 (1983); P. J. Curran, in *Plants and the Daylight Spectrum*, H. Smith, Ed. (Academic Press, London, 1981), p. 65.
17. B. N. Holben and R. S. Fraser, *Int. J. Remote Sensing* **5**, 145 (1984).
18. W. A. Allen and A. J. Richardson, *J. Opt. Soc. Am.* **58**, 1023 (1968); W. A. Allen, H. W. Gausman, A. J. Richardson, J. R. Thomas, *ibid.* **59**, 1376 (1969); H. W. Gausman, R. R. Rodriguez, A. J. Richardson, *Agron. J.* **68**, 295 (1976); C. J. Tucker, *Appl. Opt.* **16**, 1151 (1977).
19. *Special Report: Foodcrops and Shortages No. 9* (Food and Agriculture Organization, Rome, 1983), p. 12; *Sahel Weather and Crop Situation 1983, No. 6* (Food and Agriculture Organization, Rome, 1983), p. 1. Using Landsat data, D. R. Thompson and O. A. Wehmanen [*Photogramm. Eng. Remote Sensing* **45**, 201 (1979)] showed similar results for smaller areas of drought.
20. C. F. Jordan, in *Ecosystems of the World: Tropical Rain Forest Ecosystems, Structure and Function*, F. B. Golley, Ed. (Elsevier, New York, 1983), p. 117.
21. E. G. Leigh, Jr., and D. M. Windsor, in *The Ecology of a Tropical Forest: Seasonal Rhythms and Long-Term Changes*, E. G. Leigh, Jr., A. S. Rand, D. M. Windsor, Eds. (Smithsonian Institution Press, Washington, D.C., 1982), p. 111; P. A. Opler, G. W. Frankie, H. G. Baker, *J. Biogeogr.* **3**, 231 (1976); P. de T. Alvim, in *The Formation of Wood in Tropical Trees*, M. H. Zimmerman, Ed. (Academic Press, New York, 1964), p. 479.
22. A. Hladik, in *The Ecology of Arboreal Foliages*, G. G. Montgomery, Ed. (Smithsonian Institution Press, Washington, D.C., 1978), p. 51; D. M. John, *Oikos* **24**, 430 (1973).
23. H. Walter and H. Lieth, *Climate Diagram World Atlas* (Fischer, Jena, 1960-1966).
24. H. Walter, E. Harnickell, D. Mueller-Dombois, *Climate-Diagram Maps of the Individual Continents and the Ecological Climatic Regions of the Earth* (Springer, Berlin, 1975).
25. B. L. Markham, D. S. Kimes, C. J. Tucker, J. E. McMurtrey, *Photogramm. Eng. Remote Sensing* **48**, 1599 (1982).
26. J. K. Aase and F. H. Siddoway, *IEEE Trans. Geosci. Remote Sensing* **GE-19**, 78 (1981); P. J. Pinter, R. D. Jackson, S. B. Idso, R. J. Reginato, *Int. J. Remote Sensing* **2**, 43 (1981); M. D. Steven, P. V. Biscoe, K. W. Jaggard, *ibid.* **4**, 325 (1983); C. J. Tucker, B. N. Holben, J. H. Elgin, J. E. McMurtrey, *Photogramm. Eng. Remote Sensing* **46**, 657 (1980).
27. J. L. Monteith, *Philos. Trans. R. Soc. London Ser. B* **281**, 277 (1977).
28. We acknowledge a range of primary production estimates (3, 4) and the assumptions and uncertainties in extrapolation to ecosystem categories. Studies by a number of investigators (4) formed the basis for a reassessment by Ajtay *et al.* (3), who reported higher values for savanna-grassland primary production based upon much higher root production reports from this ecosystem (see also Table 1).
29. J. G. Moik, *Digital Processing of Remotely Sensed Images* (NASA, Washington, D.C., 1980).
30. J. R. G. Townshend, T. E. Goff, C. J. Tucker, in preparation.
31. We thank J. Weber, R. Money, D. Cobb, and J. Gatlin for their assistance and C. Justice and A. M. Heasty for their comments.

Prooxidant States and Tumor Promotion

Peter A. Cerutti

In cellular prooxidant states the intracellular concentration of activated forms of oxygen is increased, presumably because cells either overproduce these reactive substances or are deficient in their ability to destroy them. The major forms of active oxygen are superoxide, O_2^- , and its conjugate acid the hydroperoxy radical, HO_2^* ; singlet oxygen, O_2^1 ; the hydroxyl radical, $\cdot OH$; and hydrogen peroxide, H_2O_2 . Prooxidant states vary, depending on the type of target cell and on the induction mechanism, and can result in ubiquitous cell damage through readily oxidizable target molecules. Major reactions include initiation of autoxidation chain processes by hydroxyl and hydroperoxy radicals and of branching

reactions by alkoxy radicals, addition of hydroxyl radicals and singlet oxygen to double bonds, hydrogen abstraction from allylic carbon atoms by hydroxyl radicals, and oxidation of sulfhydryl, thioether, and amino functions (1). The biological consequences are mutations, sister chromatid exchanges, chromosomal aberrations, cytotoxicity, carcinogenesis, and cellular degeneration related to aging. In carcinogenesis active oxygen appears to play a role mostly in the promotion phase, during which gene expression of initiated cells is modulated by affecting genes that regulate cell differentiation and growth. In a subsequent step, usually referred to as progression, mostly benign neoplasms are stimulated to more rapid growth and malignancy. Active oxygen is known to induce chromosomal aberrations with high efficiency and could play a role in progression (2).

Evidence for a Role of Prooxidant States in Carcinogenesis

The human hereditary diseases ataxia telangiectasia, Fanconi's anemia, and Bloom's syndrome are characterized by increased cancer incidence and spontaneous chromosomal breakage (3). There are indications in all three diseases of abnormalities in oxygen metabolism (4). Cultured skin fibroblasts from patients with these diseases are hypersensitive to agents that induce prooxidant states. For example, fibroblasts from patients with ataxia telangiectasia are hypersensitive to x-rays, bleomycin, and neocarzinostatin; those from patients with Fanconi's anemia show sensitivity to mitomycin C and psoralen; and those from patients with Bloom's syndrome are sensitive to near-ultraviolet radiation. This last agent also induces excessive DNA strand breakage in fibroblasts from Bloom's syndrome patients. Increased oxygen tension causes excessive amounts of chromosomal aberrations in Fanconi's anemia. Serum from patients with ataxia telangiectasia and Bloom's syndrome contains clastogenic factors (CF's), and cultured fibroblasts release CF's into the culture medium. These factors break chromosomes in test cultures of lymphocytes from healthy donors. The CF from Bloom's syndrome fibroblasts was inhibited by CuZn superoxide dismutase (SOD), indicating the intermediacy of O_2^- in the clastogenic process (5). The

The author is head of the Department of Carcinogenesis at the Swiss Institute for Experimental Cancer Research, Chemin des Boveresses 155, CH-1066 Epalinges S/Lausanne, Switzerland.